

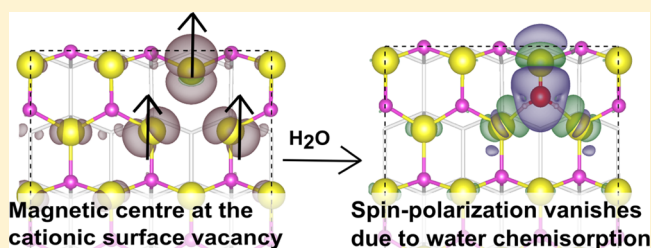
Adsorption Study of a Water Molecule on Vacancy-Defected Nonpolar CdS Surfaces

S. S. Gupta and M. A. van Huis*

Soft Condensed Matter, Debye Institute for Nanomaterials Science, Utrecht University, Princetonplein 5, 3584 CC Utrecht, The Netherlands

Supporting Information

ABSTRACT: A detailed understanding of the water–semiconductor interface is of major importance for elucidating the molecular interactions at the photocatalyst’s surface. Here, we studied the effect of vacancy defects on the adsorption of a water molecule on the (10 $\bar{1}$ 0) and (11 $\bar{2}$ 0) CdS surfaces, using spin-polarized density functional theory. We observed that the local spin polarization did not persist for most of the cationic vacancies on the surfaces, unlike in bulk, owing to surface reconstructions caused by displaced S atoms. This result suggests that cationic vacancies on these surfaces may not be the leading cause of the experimentally observed magnetism in CdS nanostructures. The surface vacancies are predominantly nonmagnetic except for one case, where a magnetic cationic vacancy is relatively stable due to constraints posed by the (10 $\bar{1}$ 0) surface geometry. At this particular magnetic defect site, we found a very strong interaction with the H₂O molecule leading to a case of chemisorption, where the local spin polarization vanishes concurrently. At the same defect site, adsorption of an O₂ molecule was also simulated, and the results were found to be consistent with experimental electron paramagnetic resonance findings for powdered CdS. The anion vacancies on these surfaces were always found to be nonmagnetic and did not affect the water adsorption at these surfaces.



INTRODUCTION

Cadmium chalcogenides (CdX, X = S, Se, Te) are II–VI semiconductors, which are used to devise solar energy harvesting solutions like thin-film photovoltaics,¹ photoelectrochemistry,² and photocatalysis.^{3,4} Over the past decade, CdS nanoheterostructures have been investigated and optimized for photocatalytic hydrogen production.³ The interface of water and the CdS nanocrystals is not well understood yet, which could be vital in deciphering the near-surface dynamics of water and its influence on surface catalysis. Any theoretical modeling of this interface should include the key interaction motifs at the surface. Some of these key surface motifs could be sought by exhaustively studying the molecular interaction of water on these surfaces, which forms the main focus of this study.

Experiments have observed an unusual ferromagnetic-like (FM) ordering in nanostructures of semiconductors and insulators, over a wide range of temperatures. This has been a subject of wide scientific interest (HfO₂,^{5,6} In₂O₃,⁶ ZnO,^{7,8} CdS^{9,10}). Such an origin of magnetism in materials, having no magnetic host ions or possible magnetic impurities, is also known as d⁰-magnetism.¹¹ Hong et al.⁶ showed that the bulk counterparts for HfO₂, In₂O₃, and TiO₂ are diamagnetic, and the FM ordering is characteristic for thin films. Later, Madhu et al.¹⁰ reported that the saturated FM ordering increases with the decrease in nanoparticle size, suggesting that surface effects may play a direct role in this phenomenon. Similar speculation that the FM mass could be concentrated at the surface was made by

studying the magnetization hysteresis loop per volume.¹² In most of these studies, it was speculated that surface vacancies (cationic or anionic), or vacancy clusters, are the cause of this widely observed FM-like behavior.

We did not find any direct experimental reports on water adsorption on CdS surfaces. However, in the late 1960s Arizumi et al. had already observed electron paramagnetic response (EPR) signals from powdered CdS single crystals.⁹ They also observed a strong interaction of H₂O on magnetic centers of powdered CdS single crystals, as they found that on exposing the paramagnetic crystals to air (water moisture) for 2 weeks, the EPR signal vanished. This is found to be qualitatively reconsolidated in our molecular study of H₂O adsorption (instead of water moisture), where we observe that a water molecule can indeed neutralize the spin polarization of a surface defect center by chemisorption. To make further comparisons with Arizumi et al. we also adsorbed an O₂ molecule at the same magnetic defect center. For a continuity in our exposition, we first discuss in full H₂O adsorption on perfect and vacancy defected surfaces, which is then followed by simulation results of this special case of O₂ adsorption and a discussion of its correspondence with experimental observations.

Received: December 27, 2016

Revised: April 20, 2017

Published: April 20, 2017

Theoretical DFT calculations using local¹³ and semilocal exchange correlational functionals^{14–16} have discussed the possibility of these magnetic cationic vacancies to be responsible for the experimentally observed FM ordering. On inclusion of more accurate theoretical treatments, like hybrid functionals,^{17,18} occupation-dependent potentials,¹⁹ and other self-interaction schemes,²⁰ it is seen that the coupling strength of such magnetic vacancies is too weak to explain the experimentally observed FM ordering. It is because they observed that the holes are more localized at the defect sites than predicted by the local and semilocal functionals. Apart from vacancy defects as a possible cause, studies have also proposed that it could be undercoordinated polar surfaces that cause the surface magnetism.^{21,22} Coey and co-workers recently made a radically different proposition, suggesting that the magnetic response of CeO₂ nanoparticles could be due to giant orbital paramagnetism emerging from the collective response of electrons in the coherent domains due to its interaction with the zero-point fluctuations of the vacuum electromagnetic field.²³ The validity of this theoretical model is yet to be confirmed by other experiments. Clearly, the understanding regarding the underlying mechanism of this FM-like behavior had shown many twists and turns and is still awaiting new developments.

In this study we do not focus on the macroscopic origin of magnetism but rather on the water-interface effects near these magnetic vacancies (which are often proposed to explain the FM-like behavior). However, we find that most of the magnetic cationic vacancies on the studied surfaces are energetically unfavorable in comparison to their nonmagnetic counterparts and may not solely be the cause of the poorly understood magnetic response of the nanostructures.

Previous theoretical studies investigating the effect on water adsorption at these magnetic vacancies did not find any case of chemisorption. Ahuja and co-workers studied the water adsorption at the defected ZnO (10 $\bar{1}$ 0) surface;²⁴ however, the prevalence of magnetic defect centers was not confirmed. They had found that the water molecules move away from the Zn vacancies and adsorb in a similar manner to the clean surface. Recently, Catellani and co-workers found a stable magnetic vacancy on the CdS (10 $\bar{1}$ 0) surface; however, its interaction with water or any other ligand was not the focus of that study.²⁵ Another adsorption study of H₂O and O₂ molecules on the clean w-CdS (10 $\bar{1}$ 0) surface was reported by the same group,²⁶ which we have used to compare with our clean surface adsorption results. In the current study, we investigate all the stable and metastable vacancies on nonpolar wurtzite CdS (w-CdS) surfaces (10 $\bar{1}$ 0) and (11 $\bar{2}$ 0), using spin-polarized density functional theory²⁷ with a semilocal exchange correlational functional. These w-CdS surfaces are the most stable and abundantly formed crystal facets, owing to their in-plane net charge neutrality. Then, we systematically study the adsorption of a water molecule on these surfaces, identifying the stable and metastable water adsorption sites. The adsorption geometries on the clean surfaces were tested by a van der Waals (vdW) functional, thus giving a benchmark for differences between the two exchange-correlational functionals. Finally, we focused on the effect of surface vacancies on the adsorption of a water molecule, highlighting the surface motifs which determine surface stability. From our study, we find that S-dimers and magnetic cationic defect centers are stabilizing surface motifs which could play a role in water adsorption; on the other hand, anion vacancies do not significantly affect it. We do not find any

case of spontaneous dissociative adsorption for the case of low coverage studied here.

■ COMPUTATIONAL METHODS

All the calculations were performed by means of density functional theory (DFT) employing the projector augmented wave (PAW) method as implemented in the VASP package.^{28,29} The equilibrium lattice parameters of the CdS unit cell were determined using the total energy minimum for a range of unit cell volumes. For each of these fixed volumes, the atoms and the cell shape were relaxed. The obtained lattice parameters ($a = 4.205$ Å, $c/a = 1.63$, $u = 0.376$) are in agreement with previous theoretical studies^{25,30} and within 2% of the experimental value.³¹ The main exchange-correlation functional used in our study is the generalized gradient approximation (GGA)-PBE,³² whereas for benchmarking tests of vdW interaction (on water adsorption) we used the vdW-optB88 functional.^{33,34}

For II–VI semiconductors it is known that considering d-states in the valence band is important for a reasonable prediction of valence band properties.³⁵ However, due to the localized nature of d-electrons, the standard DFT can only erroneously predict their binding energies. To correct for this, we included the DFT+*U* scheme³⁶ by fitting the binding energies of the d-bands to the ultraviolet and X-ray photoelectron spectroscopy data.³⁷ Using this fit, we use $U_{\text{eff}} = 6.0$ eV for the d-bands of Cd (in CdS) for the rest of the study. For the bulk supercells and surfaces the cutoff for the kinetic energy of the plane-wave basis was 400 eV, and for the augmentation charges, it was 580 eV. The Brillouin-zone integrations were performed using a Monkhorst–Pack *k*-mesh³⁸ with an electronic temperature of 0.05 eV for a Gaussian smearing at the Fermi level. Vacancy-defected bulk calculations were performed in a 128-atom wurtzite supercell with a Γ -centered *k*-point mesh of 27 irreducible *k*-points.

We modeled the nonpolar (10 $\bar{1}$ 0) and (11 $\bar{2}$ 0) surfaces with 96-atom slabs and a vacuum spacing of ~ 20 Å. The *k*-point sampling for the (10 $\bar{1}$ 0) and (11 $\bar{2}$ 0) defected surfaces used 9 and 10 irreducible *k*-points, respectively. The (10 $\bar{1}$ 0) surface was comprised of 4×3 unit cells, with a thickness of 4 bilayers (two bottom layers were fixed). The (11 $\bar{2}$ 0) surface was comprised of 2×4 unit cells with a thickness of 6 atomic layers, out of which the bottom four layers were fixed. Such a fixing of bottom layers is suitable to have a physical bulk-like termination. However, as the fixed layers are chemically noninert, this leads to undesired midgap states. For preventing these states, we passivated the fixed side of the slabs by pseudohydrogens. We used H^{1.5} ($Z = 1.5$) and H^{0.5} ($Z = 0.5$) pseudoatoms to passivate the fixed bottom layer of Cd and S atoms, respectively. The Cd–H^{1.5} and S–H^{0.5} bond lengths were determined by CdH₄^{1.5} and SH₄^{0.5} in a tetrahedral geometry. The relaxation of the surface atoms takes place in such a way that the surface anions relax outward and the cations relax inward, with respect to bulk. This is known to occur to facilitate the giving away of dangling bond electrons from surface cations to anions.

■ RESULTS AND DISCUSSION

We report and discuss the results in the following order: (a) vacancy defects (V_{Cd} and V_{S}) in bulk-CdS, (b) vacancies on nonpolar CdS surfaces, (c) adsorption of a water molecule on clean surfaces, (d) water adsorption at the vacancy defects of

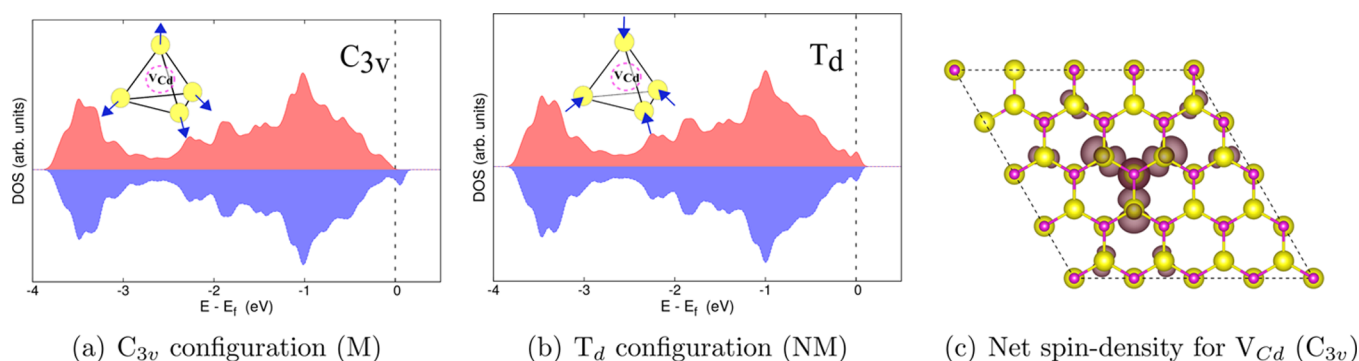


Figure 1. (a) and (b) Spin-resolved density of states for the V_{Cd} in bulk CdS and for the two cases of C_{3v} and T_d configurations, respectively (M = magnetic, NM = nonmagnetic). In (c) the net spin density is shown for the C_{3v} case, with an isosurface of $1 \times 10^{-3} e/\text{\AA}^3$. The Cd atoms are plotted in magenta and S atoms in yellow.

the surfaces, and (e) oxygen molecule adsorption at a particular cation vacancy defect.

Bulk V_{Cd} and V_S . Depending on the growth conditions, charged and neutral defects occur in the semiconductor nanostructures. In this study, we restrict our focus to the neutral vacancy defects within spin-polarized calculations, since such an adsorption study on the charged defects would be numerically prohibitive. The w-CdS cell has a lower point group symmetry than T_d , where one of the tetragonally coordinated Cd–S bonds (along c -axis) is longer than the other three equivalent bonds (by 0.007 Å for GGA-PBE). For the calculations in bulk all the atoms were relaxed, whereas the cell volume was kept constant.

The most stable state of the cation vacancy has a local magnetic moment of $2 \mu_B$, due to the localization of the holes at the neighboring S-sites. For this magnetic (M) configuration, the S-bond parallel to the c -axis is still longer than the other three equivalent S-bonds (by 0.004 Å), having a C_{3v} point group symmetry. Moreover, we also identified a metastable configuration for the cation vacancy which is nonmagnetic (NM). In this NM case, all the four neighboring S atoms relax toward the defect such that they are equidistantly located around the defect site, into a T_d point group symmetry. Such locally stable symmetric vacancy centers were also reported for CdTe and Zn-chalcogenides.^{18,19} The difference in the local structure of the cation vacancy leads to differences in the electronic structures of the neighboring S atoms, at which the hole states localize. This correlation could also be seen in the LDOS of the neighboring S atoms, as shown in Figure S1 of the Supporting Information (SI). The occurrence of two such V_{Cd} possibilities can be explained with Jahn–Teller relaxations, where the defect center with the lower symmetry (C_{3v} spin-polarized) is slightly more stable than the higher symmetry complex (T_d , nonspin-polarized). The magnetization energy of V_{Cd} and E_{mag} , i.e., the total energy difference between magnetic and nonmagnetic configurations, is just 85 meV. Figure 1(a) and (b) shows the spin-resolved density of states (DOS) of the two configurations, indicating that the C_{3v} geometry has a net spin polarization at the Fermi-level edge, whereas the T_d geometry has no net spin. Figure 1(c) shows the net spin density localized at the S atoms, which is significantly spread through the crystal. It also shows the C_{3v} nature of the spin-density symmetry and is in agreement with anisotropic spin density seen for analogous semiconductor wurtzite crystals.¹⁶ The semimetallic character seen in the DOS of Figure 1(a) and (b) has also been reported in other studies^{14–16} using local or

semilocal exchange correlational functionals. Indeed, later more accurate calculations have shown that the holes are more localized than the predictions by local or semilocal functionals;^{17,19,20} however, the local magnetic moments of the vacancy defects are often retained. Therefore, we study the adsorption on these defected surfaces within the semilocal, GGA-PBE functional level.

The sulfur vacancy in bulk CdS is found to be nonmagnetic, where the neighboring Cd atoms relax toward the defect site. The Cd-bond parallel to the c -axis is 0.04 Å longer than the other three equivalent bonds, acquiring a C_{3v} symmetry.

After studying these vacancies in bulk, it is important to know whether they are relatively stable on the surfaces. The low magnetization energy E_{mag} for the cation vacancy in bulk-CdS makes it interesting to study these defects on the nonpolar surfaces. Further, as it is believed that the experimentally observed magnetism is a surface effect, we test whether magnetism at these defect sites also persists at the surfaces.

Surface V_{Cd} and V_S . Vacancies were created on these surfaces by removing one cation/anion atom. Like in bulk-CdS, we find a variety of metastable magnetic and nonmagnetic vacancies on these surfaces. In our study, we test all possibilities by starting with different magnetic configurations as an initial condition for our calculations. Apart from the magnetic and nonmagnetic defect possibilities, there are two types of Cd and S atoms that can be accessed by an adsorbate (surface + subsurface). We thus study both such types of vacancies: the surface atoms, i.e., having coordination three are referred to as V_{Cd_1} and V_{S_1} , and the subsurface atoms with coordination of four are referred to as V_{Cd_2} and V_{S_2} .

(10 $\bar{1}0$) Surface. For the (10 $\bar{1}0$) surface the only stable V_{Cd_1} configuration is found to exhibit a net local spin, with magnetic moment of $1.62 \mu_B$. The net spin at this V_{Cd} site was also previously reported by Giacometti et al.²⁵ In our study, this is the only cationic vacancy site where a corresponding nonmagnetic configuration is not found since around this defect site the relaxation of the neighboring S atoms is restricted by surface geometry. The net spin density of V_{Cd_1} is shown in Figure 2(a). At the subsurface, the V_{Cd_2} converges to two locally stable configurations: a M solution ($1.96 \mu_B$, Figure 2(a)) and a NM solution (Figure 2(b)). Figure 2(a) and (b) show that for M V_{Cd_1} and M V_{Cd_2} , the surface relaxations near the defect sites are insignificant. On the other hand, the NM V_{Cd_2} is shown in Figure 2(c), which is accompanied by the

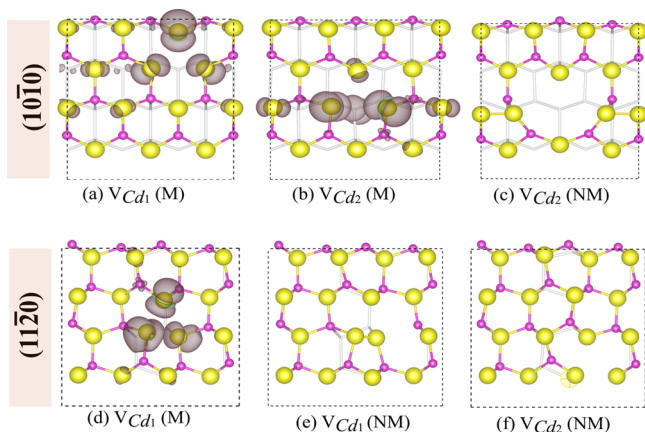


Figure 2. (a), (b), and (c) Top views of the cation-defected $(10\bar{1}0)$ surface (and subsurface); (d), (e), and (f) are the same for the $(11\bar{2}0)$ surface. The colored isosurfaces are net spin densities with an isosurface of $1 \times 10^{-3} e/\text{\AA}^3$ for the magnetic (M) cases. In the nonmagnetic (NM) cases, we can see the formation of S-dimers which stabilize the surface. The layer below (in white) is the atomic layer below the first subsurface.

formation of S-dimers. Our results repeatedly show that the surface relaxations of the neighboring anions lead to the formation of S-dimers and stabilize most of the V_{Cd} -defected surfaces, resulting into no net spin polarization at the defect site. Such relaxations of the neighboring anions are known to cause rehybridization of the hole states, leading to redistribution of the net spin density.¹³ The V_{S_1} and V_{S_2} on this surface, just like in bulk-CdS, are found to be NM.

To understand the relative likelihood of formation of the above vacancies we have compared their total energies in Figure 3(a). Here, our objective is to compare the stability of defects within the same stoichiometry (i.e., V_{Cd} -type or V_{S} -type). Therefore, it should be clear that a comparison of the relative stability of a V_{Cd} with a V_{S} is not made since that would require one to calculate chemical potentials of elemental crystals which are not reliable for DFT+ U calculations.³⁹ In Figure 3(a) the most stable V_{Cd} 's and V_{S} 's for each of the surfaces are placed lowest. Other vacancies (with the same stoichiometry) are placed in the same quadrant, with increasing energy difference from the most stable one. The M defect configurations are marked in green and the NM in black. In Figure 3(a), we observe that the magnetic V_{Cd_2} is 0.59 eV less stable than its NM counterpart V_{Cd_2} . Moreover, this subsurface Cd-vacancy (V_{Cd_2}) is even more stable than the surface Cd-vacancy (V_{Cd_1}) by 85 meV, thus highlighting the stabilizing role of S-dimers formed on nonmagnetic V_{Cd_2} . It should be noted that according to Figure 3(a) V_{Cd_1} is the only magnetic defect site which is relatively stable on these surfaces. The V_{S_1} on $(10\bar{1}0)$ is easier to be formed by 0.6 eV than the subsurface V_{S_2} , which is in accordance with their coordination number. Since V_{S} does not occur in a variety of magnetic states and do not interact strongly with water, their surface geometries are discussed in their respective section of water adsorption.

$(11\bar{2}0)$ Surface. As the $(11\bar{2}0)$ surface is more open for relaxations, it favors NM ground states for cation vacancies. The stable NM configurations are shown in Figure 2(e) and (f) for V_{Cd_1} and V_{Cd_2} . A magnetic V_{Cd_1} was also observed which is

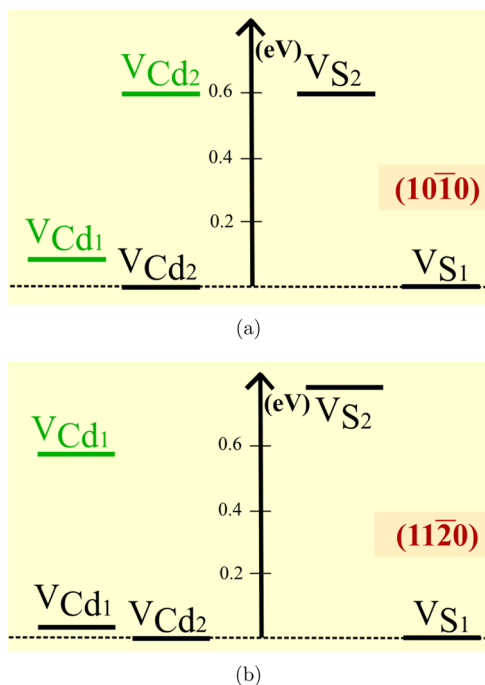


Figure 3. (a) and (b) Summarize the relative stability for the vacancies with the same stoichiometry on the $(10\bar{1}0)$ and $(11\bar{2}0)$ surfaces. The most stable Cd-type and S-type defects are placed lowest (set to zero on the vertical axis). Magnetic vacancies are displayed in green and nonmagnetic vacancies in black.

shown in Figure 2(d), with its net spin-density ($2 \mu_{\text{B}}$). As shown in Figure 2(e) and (f), in the case of NM V_{Cd_1} the dimer is formed with the surface S atoms, while for NM V_{Cd_2} it forms with the next subsurface atomic layer. These dimer-S states have $d_{\text{S-S}} = 2.12 \text{ \AA}$, which is shorter in comparison to $d_{\text{Cd-S}}$ for a clean unrelaxed surface which is 2.57 \AA . A relative thermodynamical stability of these defects is shown in Figure 3(b), where the M V_{Cd_1} is 0.57 eV less stable than NM V_{Cd_1} . No metastable magnetic state was found for V_{Cd_2} . The V_{S} 's are again found to be NM. Figure 3(b) shows that the likelihood of formation for V_{S} 's are again in accordance with their coordination number, where the V_{S_1} is 0.79 eV more stable than V_{S_2} .

In summary, we observed that magnetic vacancies do not form stable ground states on these nonpolar surfaces, except for V_{Cd_1} on the $(10\bar{1}0)$ surface, which is relatively stable. This is because the neighboring anion relaxations are easier to occur for the nonpolar surfaces, leading to rehybridization of the orbitals localizing the defect states, and cause the vanishing of the local spin polarization. In the following section, we present results of water adsorption on all the vacancy defects at these surfaces to understand all the possible interactions with water. First, we focus on the adsorption at the clean surface, followed by adsorption at the vacancy-defected surfaces.

Adsorption of Water Molecule on the Surfaces. We began by investigating possible adsorption sites of a single water molecule on the clean $(10\bar{1}0)$ and $(11\bar{2}0)$ surfaces. Since these surfaces are nonpolar they have more than one adsorption motif. We report below the most stable and metastable adsorption configurations on the two surfaces.

(10 $\bar{1}0$) Surface. After spanning several initial geometries of H₂O adsorption on this surface, four configurations were found to be (meta-)stable. Among these, the most stable adsorption configuration is at the *hollow site* as shown in Figure 4(a), with

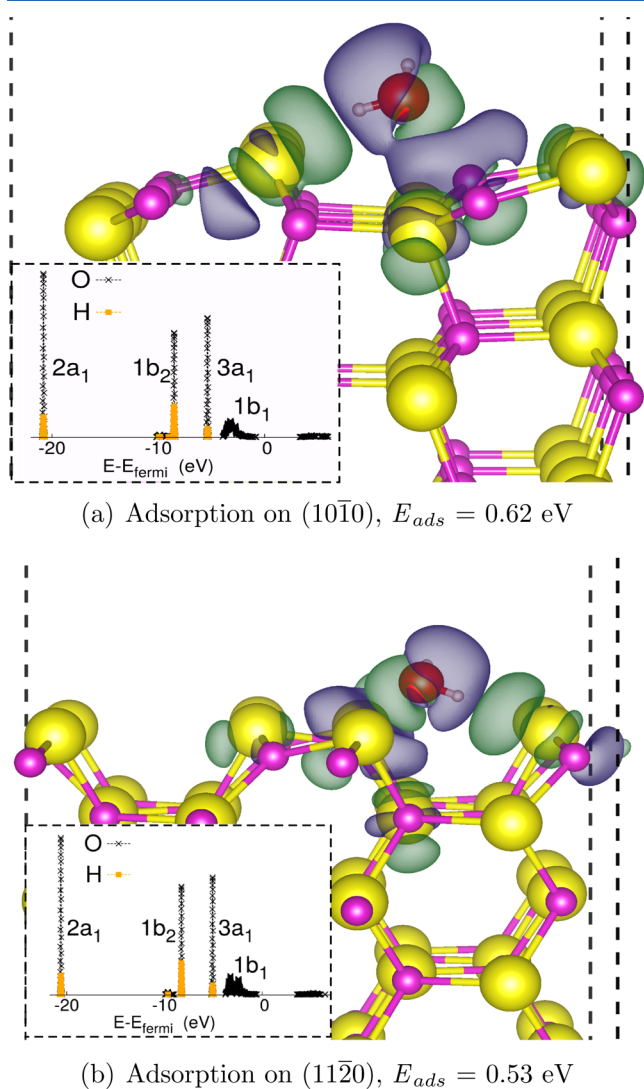


Figure 4. (a) Charge difference density plot of the most stable H₂O adsorption configuration on the clean (10 $\bar{1}0$) surface and the (b) same for the (11 $\bar{2}0$) surface. An isosurface of charge density of $4.7 \times 10^{-4} e/\text{\AA}^3$ is used where the blue color indicates charge depletion and green indicates charge accumulation. The inset shows the LDOS for the H₂O molecule, which indicates the case of physical adsorption.

$E_{ads} = 0.62$ eV. When the input water geometry was altered by orienting the H–O–H planes parallel or perpendicular to the surface, the adsorbed molecule relaxed to the same geometry, within a difference of 5 meV in E_{ads} . At this site both possible bonding interactions ($d_{Cd-O} \sim 2.4$ Å, $d_{S-H} \sim 2.3$ Å) took place. The inset shows the LDOS for the H₂O molecule, where the molecular orbitals of water have remained intact and the 1b₁ O-states have become dispersed, indicating a physical adsorption at this surface. This adsorbed configuration was also seen in an earlier study;²⁶ however, their value of $E_{ads} = 0.33$ eV is significantly lower than in our calculations. This could be the result of small supercell sizes (2 × 1) used for their study.

The other three metastable adsorption configurations are shown in Figure 5(a), (b), and (c). These metastable

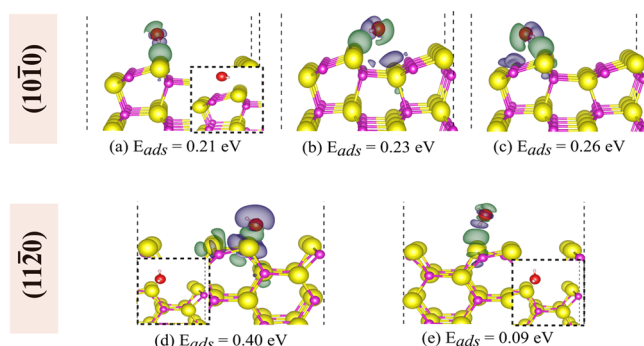


Figure 5. (a), (b), (c) are the charge density difference plots for metastable geometries of adsorption of the H₂O molecule on (10 $\bar{1}0$) surface, and (d) and (e) are the same for the (11 $\bar{2}0$) surface. An isosurface of charge density of $4.7 \times 10^{-4} e/\text{\AA}^3$ is used. The insets in (a), (d), and (e) show the change in geometry upon relaxing with the vdW-optB88 functional; (b) and (c) do not show any changes in their geometry.

possibilities were not previously reported. These locally converged configurations were obtained through a rotation of the H–O–H plane of the molecule, about the neighboring S atom. By doing this, the Cd–O bonding interaction increases only slightly (as shown by the charge difference density plots), leading to a difference in E_{ads} of 50 meV. This indicates that the potential energy surface for the (10 $\bar{1}0$) is very flat around these geometries. The strength of the S–H interactions in physisorption could be estimated to be ~ 0.1 eV since the configuration (a) is bonded only through these interactions (2S–H bonds). The insets represent the converged vdW geometries, which we discuss later.

(11 $\bar{2}0$) Surface. Unlike the (10 $\bar{1}0$) surface, the (11 $\bar{2}0$) is ridged and far from being flat. The most stable adsorption configuration on this surface is also at the *hollow* position as shown in Figure 4(b), with an $E_{ads} = 0.53$ eV. The inset shows the LDOS for the adsorbed water molecule, indicating intact molecular orbitals of water and dispersed 1b₁ levels of the O atom. Other metastable configurations at this surface are shown with their charge difference density plots in Figure 5(d) with $E_{ads} = 0.40$ eV and (e) with $E_{ads} = 0.09$ eV. Owing to the ridged surface, the difference in their E_{ads} is also significant.

Effect of vdW Interaction. Since the H₂O molecule and the nonpolar surfaces are likely to have dipole interactions, it is important to estimate the strength of vdW interactions. For this purpose, in addition to the GGA-PBE functional, we also used the vdW-optB88^{33,34} functional for all the adsorption geometries on the clean surface. To investigate the effect of vdW interaction on E_{ads} and relaxed geometries, we performed the vdW calculations on the same input geometries that were used for PBE calculations, keeping the dimensions of the cell constant (while allowing the relaxation of atoms that were also free to relax in the PBE calculations). Table 1 shows the E_{ads} for the vdW and PBE functionals for the geometries shown in Figure 4 and Figure 5. We found that there is no significant change in geometry for the most stable configurations of both the surfaces, i.e., configurations Figure 4(a) and (b). When vdW interactions are taken into account, the E_{ads} increases for both these cases by 0.17 eV.

On including dispersion interaction the configuration of Figure 5(a) is not the least stable anymore, and it converges to the configuration of Figure 5(c) (as indicated in the inset). As the other two metastable cases of the (10 $\bar{1}0$) surface (Figure

Table 1. Effect of vdW Functional on the Adsorption Geometry and Energies

	$E_{\text{ads}}^{\text{PBE}}$ (eV)	$E_{\text{ads}}^{\text{vdW}}$ (eV)
(10 $\bar{1}0$)		
Figure 4(a)	0.62	0.79
Figure 5(a)	0.21	0.39 ^a
Figure 5(b)	0.23	0.36
Figure 5(c)	0.26	0.39 ^a
(11 $\bar{2}0$)		
Figure 4(b)	0.53	0.70
Figure 5(d)	0.40	0.68 ^a
Figure 5(e)	0.09	0.68 ^a

^aConverged to the same geometry.

5(b) and (c)) do not show any significant change in the adsorption geometry, we can infer that the vdW effect on the (10 $\bar{1}0$) surface increases the E_{ads} by ~ 0.15 eV. For the ridged (11 $\bar{2}0$) surface, inclusion of dispersion interaction can lead to relaxation of the H₂O molecule toward the hollow site of the surface. In other words, for the configurations on this surface which were metastable with the PBE functional, the inclusion of vdW interaction can lead to adsorption which is nearly as strong as the most stable configuration of the (11 $\bar{2}0$) surface, i.e., Figure 4(b). This is also what we observe in our findings, where the final geometry upon vdW relaxation is shown in the insets of Figure 5(d) and (e). The water molecule in Figure 5(d) is altered in its geometry by a rotation of the H–O–H plane over the surface ridge to fall into the hollow site, leading to an enhanced bonding with the surface which explains a larger increase in the E_{ads} of 0.28 eV. The least stable configuration of Figure 5(e) was also no longer locally stable and relaxed to its inset figure, which is similar to the vdW-converged case of the Figure 5(d) configuration.

This benchmarking gives an estimate of the possible effect on geometries and E_{ads} due to vdW remarkably interaction, indicating that for the ridged (11 $\bar{2}0$) surface the metastable configurations converge to the most stable configurations. Despite the substantial changes seen in the adsorption on the pristine (11 $\bar{2}0$) surface, it should be noted that we have taken into account the vdW interaction for the clean surface adsorption only. This is because of the fact that most of the currently used vdW functionals consider only the total density (spin \uparrow + spin \downarrow) of the system and, in this way, are unsuitable for the treatment of spin-polarized systems.^{34,40} All the results on the defected surfaces discussed below were obtained for the PBE exchange correlational functional.

One of the main objectives of this study is to investigate the effect of vacancies on the surface adsorption of H₂O, which are discussed below for both the M and NM vacancies. In addition to this, we have also studied a case of O₂ adsorption at one particularly stable magnetic vacancy site to compare with the observations of Arizumi et al. The results and comparison of this set of calculations with experiments are reported in the last section of Results and Discussion, while we start with a discussion of the water molecule adsorption results.

Adsorption on Surface V_{Cd} and V_{S} . At the Magnetic Vacancy Sites. The three (meta-)stable magnetic cation vacancies were found for V_{Cd_1} and V_{Cd_2} on the (10 $\bar{1}0$) surface and for V_{Cd_1} on the (11 $\bar{2}0$) surface (Figure 2(a), (b), (d)). We then initialized the adsorption calculation with the water molecule exactly above these defect sites.

V_{Cd_1} on (10 $\bar{1}0$). At this site we found two cases of H₂O adsorption. The most interesting case was found for an initial guess of a nonmagnetic solution, where the water molecule is chemisorbed as shown in Figure 6. Here, after relaxation the

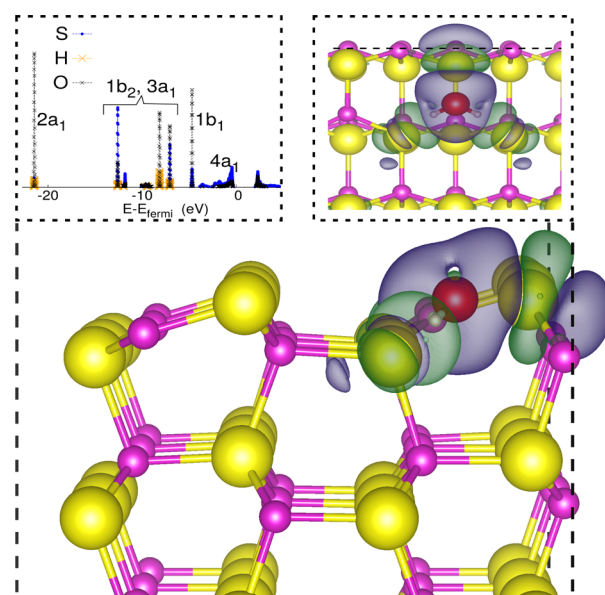


Figure 6. The above configuration represents the interaction of water with the magnetic cation vacancy site leading to chemisorption ($E_{\text{ads}} = 1.48$ eV), where the water molecule becomes a part of the surface. Chemisorption of H₂O at the (10 $\bar{1}0$) V_{Cd_1} site leads to neutralizing of the surface magnetic moment. The inset on the left shows the local DOS of the adsorbed H₂O and the surface-S site to which the molecule is bonded, which shows the splitting of H₂O molecular orbitals (1b₂ and 3a₁) and forming of new O–S bonds instead. The inset on the right shows a top view of the charge density difference plot (isosurface = 10^{−3} e/Å³), where it is seen that the symmetry of the surface assists the H₂O to bond.

local magnetic moment of the surface eventually vanished, with significantly higher E_{ads} at 1.48 eV. Figure 6 shows that the H₂O molecule became a part of the surface, as a new O–S bond was formed with bond length $d_{\text{O–S}} = 1.76$ Å, accompanied by an increase in the water $d_{\text{O–H}}$ bonds by 12.8%. The sulfur monoxide bond in the same settings has a bond length of $d_{\text{O–S}} = 1.50$ Å, comparable to what we observe for the O_{H₂O}–S_{CdS} bond. The adsorbed $\angle\text{H–O–H}$ is 103°, while the surface $\angle\text{S–Cd–S}$ is 114.9°. The top right inset of Figure 6 shows this good match, where H₂O fits well with the symmetry of the surface. The top left inset of Figure 6 shows the LDOS of H and O from the H₂O molecule and of the surface-S bonded to the molecule. Here, the 1b₂ and 3a₁ water molecular orbitals undergo splitting, thereby forming new O–S bonds with these states. New 4a₁-like O states are seen at the valence band edge and the conduction band edge, where they bond with the surface-S, clearly establishing new bonding patterns.

It is interesting that the local spin polarization at the surface can be neutralized by a chemisorption process of a diamagnetic ligand (like water, in this case). This finding is in qualitative agreement with experimental reports of Arizumi et al.,⁹ where it was observed that long exposure to moisture in the air can diminish the EPR signal from the paramagnetic centers of the CdS single crystals. To compare more directly with Arizumi et al., we performed additional simulations where an oxygen

molecule was adsorbed over this relatively stable magnetic defect center (V_{Cd_1}). An account of our results of O_2 adsorption at this stable magnetic defect center are discussed in the last section of the [Results and Discussion](#). Our results are consistent with the EPR reports by Arizumi et al., where we observe that the adsorption strength of the paramagnetic oxygen molecule is lower ($E_{ads}^{O_2} = 0.47$ eV, [Figure 9](#) in the last section) than that of the diamagnetic water molecule at the magnetic centers. However, we cannot detailedly compare our specific case of water chemisorption to the experimental results since in the latter the interaction with water moisture (and not the gaseous phase) is considered. Because of this difference, while we find a clear case of chemisorption of a water molecule, in experiments the EPR signal gradually appeared on heating at 100 °C, indicating lower adsorption energy of water moisture. This is reasonable since the liquid water phase would certainly have lower bonding strengths with the surface than the isolated chemisorped molecule case which we have studied.

Another metastable adsorption configuration at this site was found, whereby the net local spin at the defect site persists and allows a very weak adsorption of the water molecule ($E_{ads} = 0.08$ eV). Apparently, for this metastable solution the interaction between the defect spin density and an overlying water molecule is repulsive since its E_{ads} is much smaller than the least stable adsorption configuration of the clean surfaces. To verify this, we rotated the orientation of the H–O–H plane away from the spin densities, where we indeed observed an increase in E_{ads} to 0.19 eV. Such a low E_{ads} of the metastable solution, in comparison to the chemisorped geometry, ensures that the former would not be occurring in practice.

V_{Cd_2} on $(10\bar{1}0)$. The adsorption process at this magnetic site converges to a stable state ($E_{ads} = 0.30$ (1.04) eV) where the neighboring S atoms form dimer-S states with the subsurface layers, as shown in [Figure 7\(a\)](#). The calculation of $E_{ads} = 0.30$ eV accounts only for the interaction strength where the E_{ads} is comparable with the clean surface. The value in the parentheses also includes the surface stabilization energy upon relaxation, at 1.04 eV. The difference in these two values is the surface stabilizing contribution of the stable NM surface in comparison to the initial metastable M configuration. In [Figure 7\(a\)](#) H_2O is seen to adsorb with the S-dimer states at the surface. It is to be noted that in the presence of water it does not converge to the NM V_{Cd_2} , as observed earlier in [Figure 2\(c\)](#), but to a new way of forming S-dimers with the subsurface layer, again neutralizing the locally polarized spin. This shows that the physical inclusion of water for adsorption induces relaxations at the surface, which drive the metastable M V_{Cd_2} to a new NM V_{Cd_2} .

V_{Cd_1} on $(11\bar{2}0)$. Upon adsorption of a water molecule at this site, the only magnetic metastable site at the $(11\bar{2}0)$ surface ([Figure 2\(d\)](#)) relaxed to the NM case of V_{Cd_1} on $(11\bar{2}0)$, analogous to [Figure 2\(e\)](#). This will be discussed with the cases of NM defect adsorption in the following section. Another metastable water adsorption solution at this site is observed where the local spin moment persists, leading to another case of very weak adsorption ($E_{ads} = 0.12$ eV). As expected, this magnetic case did not exhibit any surface reconstruction.

At Nonmagnetic Vacancy Sites. We also adsorbed a water molecule at NM vacancy sites on the two surfaces. For the V_{Cd} , these sites were [Figure 2\(c\)](#), (e), and (f). Their respective adsorption geometries are shown in [Figure 7\(b\)](#), (c), and (d).

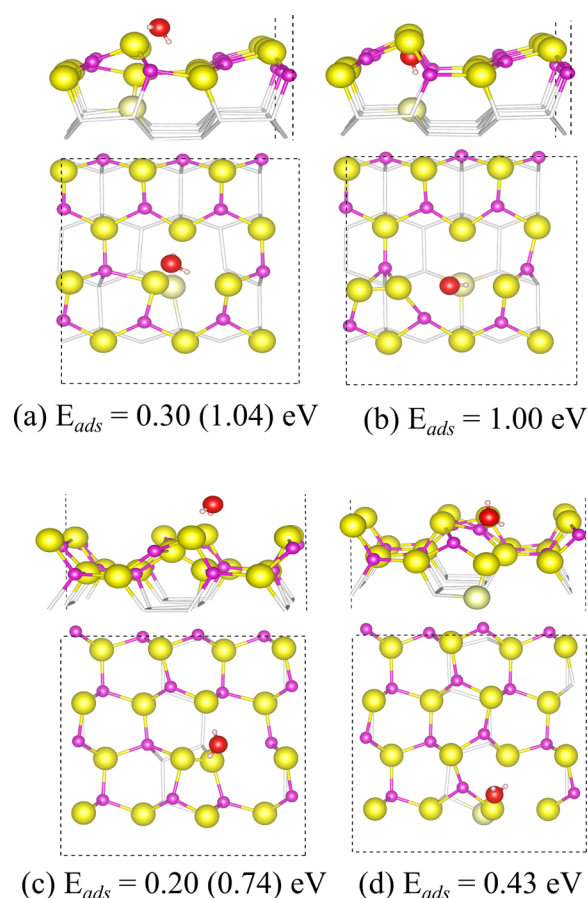


Figure 7. (a) and (b) Show the adsorption geometries for a water molecule on M and NM in the case of V_{Cd_2} on $(10\bar{1}0)$. (c) and (d) show the same for NM cases of V_{Cd_1} and V_{Cd_2} of the $(11\bar{2}0)$ surface.

For the ease of comparison between the two figures, we have also shown the M case of V_{Cd_2} of the $(10\bar{1}0)$ surface in [Figure 7\(a\)](#), which was already discussed in the previous section. In the open cage-like site of [Figure 2\(b\)](#), the water molecule is *trapped* as shown in [Figure 7\(b\)](#), where it is seen to adsorb slightly below the surface atomic layer. The high adsorption strength of this configuration is due to the interaction of H_2O with three surface motifs—two S-dimer sites and the subsurface S atom. [Figure 7\(c\)](#) is the converged adsorption geometry for both the M case of [Figure 2\(d\)](#) and the NM case of [Figure 2\(e\)](#), with an $E_{ads} = 0.20$ (0.74) eV. Again, 0.20 eV accounts for the actual adsorption strength, while the value in the parentheses accounts to stabilizing energy of the NM surface. This low adsorption interaction is comparable to the strength of S–H bonds on the clean surface. [Figure 7\(d\)](#), the adsorption case of [Figure 2\(f\)](#), shows an adsorption strength of 0.43 eV, with H_2O adsorbing at the dimer-S site.

At V_S Sites. The adsorbed geometries at the V_S of the $(10\bar{1}0)$ and $(11\bar{2}0)$ surfaces are shown in [Figure 8\(a, b\)](#) and (c, d), respectively. For V_{S_1} on both the surfaces, in [Figure 8\(a\)](#) and (c), the H_2O moved away from the sulfur vacancy and converged close to the nearest Cd atom or S atom for physical adsorption. The V_{S_2} in [Figure 8\(b\)](#) and (d) forms an open-ring structure where the H_2O adsorbs. Overall, the E_{ads} at the V_S sites are similar to those at the clean surfaces, indicating that the S-vacancy has almost no effect on the adsorption of water.

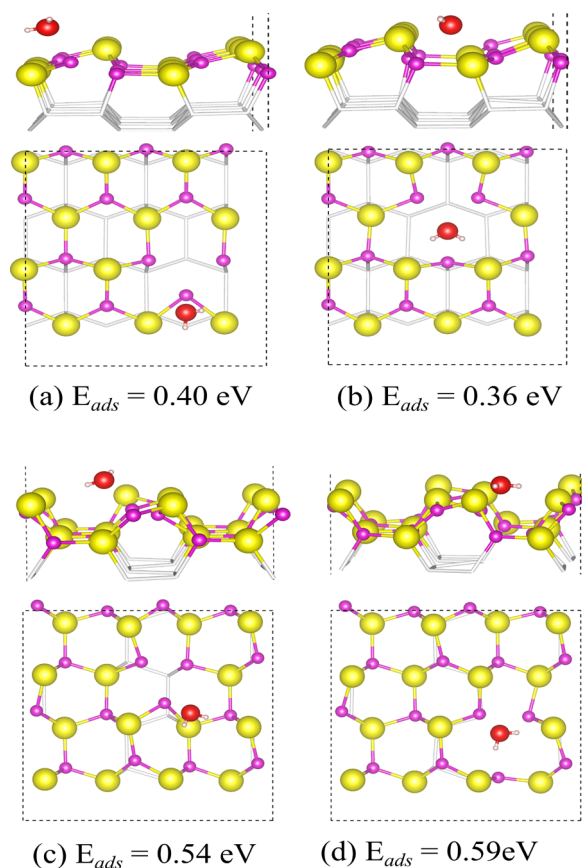


Figure 8. (a), (b) H₂O adsorption geometries on V_{S_1} and V_{S_2} defects of the $(10\bar{1}0)$ surface, and (c) and (d) are the same for the $(11\bar{2}0)$ surface.

Adsorption of O₂ the Molecule on the V_{Cd_1} Defect of the $(10\bar{1}0)$ Surface. To make a comparative assessment with the H₂O and O₂ adsorption, as described in the experimental report of ref 9, we also studied the adsorption of an O₂ molecule at the stable magnetic defect center (V_{Cd_1}) of the $(10\bar{1}0)$ surface. The same computational settings (GGA-PBE, energy cutoff, k-points) were used as in the H₂O adsorption calculations. The isolated O₂ molecule (serving as a reference for calculating E_{ads}) was calculated in a cubic box of 20 Å in length. The O–O bond length of the O₂ molecule was 1.23 Å, with a magnetic moment of $2 \mu_B$.

Figure 9 briefly summarizes the observed metastable and stable adsorption configurations of the O₂ molecule at the V_{Cd_1} site on the $(10\bar{1}0)$ surface. The state in column (a) is paramagnetic where the oxygen molecule does not interact with the spin density at the defect site. The electronic levels of atoms O₁ and O₂ are unaffected by the surface, in the second row of column (a), leading to an E_{ads} of 0.01 eV. Also, the net spin densities (shown in the third row of column (a)) are almost unchanged owing to very little interaction. The configuration in column (b) is a nonmagnetic solution. Here, the electronic states of the oxygen molecule (shown by atoms O₁ and O₂) and the S atom of the surface (bonded to the molecule) align with one another, resulting in a considerable interaction with $E_{ads} = 0.28$ eV. In this case, as both the local and overall spin polarizations are zero, the net spin density plot is not shown. Column (c) of Figure 9 shows the most stable of the oxygen adsorption geometries with $E_{ads} = 0.47$ eV, having the geometry

very similar to case (b). The second row of column (c) shows that electronic levels of O₁ and surface-S undergo splitting near the valence band and conduction band edges, leading to a stronger adsorption. The net spin density plot of geometry (c) indicates that the spin polarizations at the oxygen molecule and at the defect site are directed opposite to one another. The local magnetic moments at the molecule are $m^{O_1} = 0.30 \mu_B$ and $m^{O_2} = 0.46 \mu_B$, while the surface S atoms have magnetic moments with values between $-0.2 \mu_B$ and $0.0 \mu_B$, resulting in a net moment of $0.29 \mu_B$ in the cell.

These results of the most stable O₂ molecule adsorption geometry on the V_{Cd_1} defect site (column (c)), along with the case of water chemisorption on the same site, are consistent with the experimental findings of ref 9. First, the surface adsorption of a H₂O molecule at the magnetic defect center is ~ 1 eV stronger than that of O₂ adsorption. The experiments have shown that water moisture can replace the O₂ molecule from surface adsorption. At least for the case of the isolated water molecule considered here, the difference in adsorption energy is significantly large and consistent with this finding. Second, for both the cases (b) and (c), the O₂ adsorption geometries result in a decrease of the local spin polarization of the magnetic defect center of the surface. For the most stable case of column (c), the overall magnetic moment of the cell reduced to $0.29 \mu_B$ (which was initially about $1.62 \mu_B$ for the surface vacancy, before adding O₂). For both H₂O and O₂ adsorption at this V_{Cd_1} defect site diminishes its spin polarization. Third, the experiment observed a broadening in the magnetic resonance lines, which was shown to be a result of the dipolar interaction between the O₂ molecule and the paramagnetic center on the surface. This scenario shown in column (c) in Figure 9 fits well with this finding, as the LDOS and net spin density plots show that the local spin polarizations are directed opposite to one another, leading to dipolar interactions.

Keeping in mind our prediction of thermodynamic stability leading to a predominance of nonmagnetic cationic vacancies on these surfaces, we would like to clearly state our inferences in relation to the experiments. Although our results are recurrently consistent with some of the observations of Arizumi et al., we do not claim that the V_{Cd_1} is the source of magnetic signal observed experimentally with powdered CdS or the CdS nanostructures (observed in the past decade). Such a prediction of the magnetic origin can only be confirmed by a theoretical macroscopic prediction of correlated magnetism, which we have not covered here. However, we show that simple vacancies like V_{Cd_1} could prove to be a suitable testbed for studying localized adsorption interactions at d⁰ magnetic centers of the semiconductor surfaces.

CONCLUSION

We have extensively studied water adsorption at the neutral vacancies of nonpolar w-CdS surfaces, with all of their possible magnetic configurations. First, we have shown that most of the vacancies on these nonpolar surfaces are nonmagnetic. The net spin polarization is relatively unstable, owing to possible surface relaxations which result in stable anion dimers. This finding indicates that whenever the surface geometry is not structurally constrained and relaxations are likely to occur, the stable vacancy configurations would be NM. Hence, most of the cationic vacancies (i.e., one out of four) on the nonpolar CdS

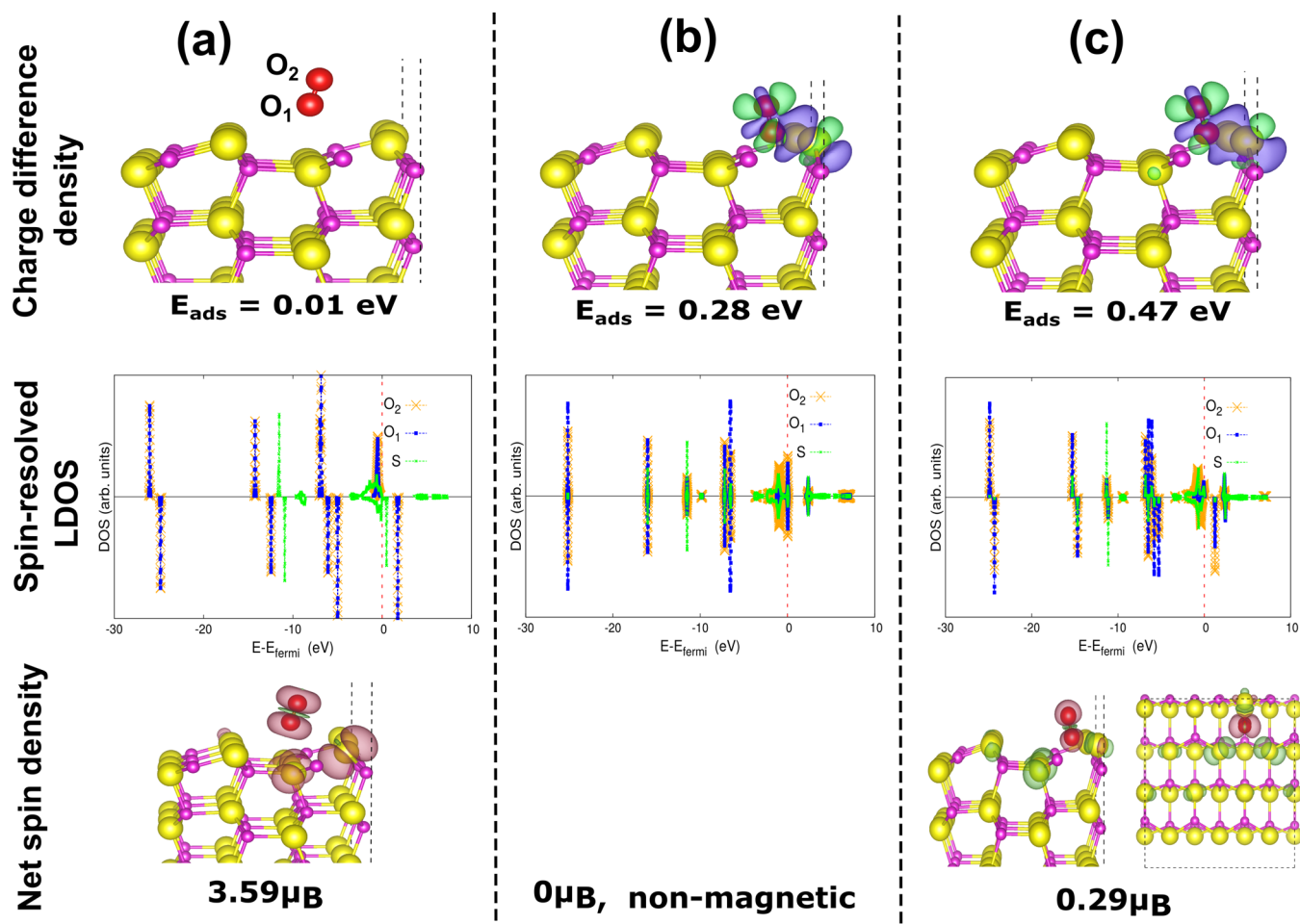


Figure 9. Columns (a), (b), and (c) represent the characteristics of the converged geometries that were obtained for the O_2 molecule adsorption at the V_{Cd1} magnetic site on the $(10\bar{1}0)$ surface. The two O atoms of the oxygen molecule are referred to as O_1 and O_2 atoms of the molecule, as shown in geometry (a). The first row indicates their respective charge difference plots of the configurations. The second row shows the spin-resolved LDOS for the configurations, indicating the two O atoms and surface S atom which bonds to the molecule. The third row shows the net spin density for these configurations. In the nonmagnetic case of (b) the local and the spin densities are zero and not shown here.

surfaces do not exhibit a thermodynamically stable magnetic moment, and therefore the vacancies from these surfaces may not solely be the cause of the experimentally observed FM behavior. Second, we have shown that for one of the relatively stable vacancy sites, where the neighboring atom relaxations are structurally constrained, a relatively stable magnetic cationic vacancy is the only possibility. Upon adsorption of a water molecule on such a stable magnetic site, we found a clear case of chemisorption. In this case, the water molecule strongly interacts with the surface, resulting in no net spin polarization. For comparison with an experimental report,⁹ we also adsorbed an O_2 molecule at this interesting surface vacancy. The O_2 adsorption resulted in a decrease in the local magnetic moment, although with lower adsorption energy in comparison to H_2O . These relative adsorption strengths, diminishing of the magnetic signal, and the dipolar interaction of O_2 adsorption are all consistent with the EPR findings. For other nonmagnetic cationic vacancy cases, the surface motifs like S-dimers or the subsurface-S atoms can be the main interaction centers for the H_2O molecule. For the interaction with the S-dimers, the adsorption energies are comparable to or lower than those of the clean surfaces. Unlike the cation vacancies, the anion vacancies do not significantly affect the H_2O adsorption in comparison to clean surface adsorption.

■ ASSOCIATED CONTENT

📄 Supporting Information

The Supporting Information is available free of charge on the ACS Publications website at DOI: 10.1021/acs.jpcc.6b13010.

(I) Local DOS of S atoms neighboring the V_{Cd} in bulk CdS (PDF)

■ AUTHOR INFORMATION

Corresponding Author

*E-mail: m.a.vanhuis@uu.nl.

Notes

The authors declare no competing financial interest.

■ ACKNOWLEDGMENTS

S.S.G. would like to thank Wun Fan Li and Xiaobin Xie for helpful discussions and comments on the manuscript. M.A.v.H. acknowledges support from The Netherlands Organization for Scientific Research (NWO) for a VIDI (Grant No. 723.012.006) and from the European Research Council (ERC Consolidator Grant No. 683076 NANO-INSITU). This work is part of the Industrial Partnership Programme “Computational Sciences for Energy Research” (Grant No. 13CSER067)

of the NWO-I. This research program is cofinanced by Shell Global Solutions International B.V.

REFERENCES

- (1) Morales-Acevedo, A. Thin Film CdS/CdTe Solar Cells: Research Perspectives. *Sol. Energy* **2006**, *80*, 675–681. {SREN} '05 - Solar Renewable Energy News Conference.
- (2) Emin, S.; Fanetti, M.; Abdi, F. F.; Lisjak, D.; Valant, M.; van de Krol, R.; Dam, B. Photoelectrochemical Properties of Cadmium Chalcogenide-Sensitized Textured Porous Zinc Oxide Plate Electrodes. *ACS Appl. Mater. Interfaces* **2013**, *5*, 1113–1121.
- (3) Chen, X.; Shen, S.; Guo, L.; Mao, S. S. Semiconductor-Based Photocatalytic Hydrogen Generation. *Chem. Rev.* **2010**, *110*, 6503–6570.
- (4) Amirav, L.; Alivisatos, A. P. Photocatalytic Hydrogen Production with Tunable Nanorod Heterostructures. *J. Phys. Chem. Lett.* **2010**, *1*, 1051–1054.
- (5) Venkatesan, M.; Fitzgerald, C. B.; Coey, J. M. D. Thin Films: Unexpected Magnetism in a Dielectric Oxide. *Nature* **2004**, *430*, 630–630.
- (6) Hong, N. H.; Sakai, J.; Poirot, N.; Brizé, V. Room-Temperature Ferromagnetism Observed in Undoped Semiconducting And Insulating Oxide Thin Films. *Phys. Rev. B: Condens. Matter Mater. Phys.* **2006**, *73*, 132404.
- (7) Khalid, M.; Ziese, M.; Setzer, A.; Esquinazi, P.; Lorenz, M.; Hochmuth, H.; Grundmann, M.; Spemann, D.; Butz, T.; Brauer, G.; et al. Defect-Induced Magnetic Order in Pure ZnO Films. *Phys. Rev. B: Condens. Matter Mater. Phys.* **2009**, *80*, 035331.
- (8) Podila, R.; Queen, W.; Nath, A.; Arantes, J. T.; Schoenhalz, A. L.; Fazzio, A.; Dalpian, G. M.; He, J.; Hwu, S. J.; Skove, M. J.; et al. Origin of FM Ordering in Pristine Micro- and Nanostructured ZnO. *Nano Lett.* **2010**, *10*, 1383–1386.
- (9) Arizumi, T.; Mizutani, T.; Shimakawa, K. EPR Study on Surface Properties of ZnS and CdS. *Jpn. J. of Appl. Phys.* **1969**, *8*, 1411.
- (10) Madhu, C.; Sundaresan, A.; Rao, C. N. R. Room-Temperature Ferromagnetism in Undoped GaN And CdS Semiconductor Nanoparticles. *Phys. Rev. B: Condens. Matter Mater. Phys.* **2008**, *77*, 201306.
- (11) Coey, J. ferromagnetism. *Solid State Sci.* **2005**, *7*, 660–667. A tribute to Erwin Felix Bertaut.
- (12) Khalid, M.; Setzer, A.; Ziese, M.; Esquinazi, P.; Spemann, D.; Pöppel, A.; Goering, E. Ubiquity of Ferromagnetic Signals in Common Diamagnetic Oxide Crystals. *Phys. Rev. B: Condens. Matter Mater. Phys.* **2010**, *81*, 214414.
- (13) Das Pemmaraju, C.; Sanvito, S. Ferromagnetism Driven by Intrinsic Point Defects in HfO₂. *Phys. Rev. Lett.* **2005**, *94*, 217205.
- (14) Osorio-Guillén, J.; Lany, S.; Barabash, S. V.; Zunger, A. Magnetism without Magnetic Ions: Percolation, Exchange, and Formation Energies of Magnetism-Promoting Intrinsic Defects in CaO. *Phys. Rev. Lett.* **2006**, *96*, 107203.
- (15) Dev, P.; Zhang, P. Unconventional Magnetism in Semiconductors: Role of Localized Acceptor States. *Phys. Rev. B: Condens. Matter Mater. Phys.* **2010**, *81*, 085207.
- (16) Volnianska, O.; Boguslawski, P. High-Spin States of Cation Vacancies In GaP, GaN, AlN, BN, ZnO, and BeO: A First-Principles Study. *Phys. Rev. B: Condens. Matter Mater. Phys.* **2011**, *83*, 205205.
- (17) Wang, X.; Zhao, M.; He, T.; Wang, Z.; Liu, X. Can Cation Vacancy Defects Induce Room Temperature Ferromagnetism In GaN. *Appl. Phys. Lett.* **2013**, *102*, 062411.
- (18) Shepidchenko, A.; Sanyal, B.; Klintonberg, M.; Mirbt, S. Small Hole Polaron In CdTe: Cd-Vacancy Revisited. *Sci. Rep.* **2015**, *5*, 14509.
- (19) Chan, J. A.; Lany, S.; Zunger, A. Electronic Correlation in Anion *p*-orbitals Impedes Ferromagnetism Due To Cation Vacancies in Zn Chalcogenides. *Phys. Rev. Lett.* **2009**, *103*, 016404.
- (20) Droghetti, A.; Pemmaraju, C. D.; Sanvito, S. Predicting d⁰ Magnetism: Self-Interaction Correction Scheme. *Phys. Rev. B: Condens. Matter Mater. Phys.* **2008**, *78*, 140404.
- (21) Tang, J.-P.; Wang, L.; Luo, H.-J.; Xiao, W.-Z. Magnetic Properties in Zinc-Blende CdS Induced by Cd Vacancies. *Phys. Lett. A* **2013**, *377*, 572–576.
- (22) Fischer, G.; Sanchez, N.; Adeagbo, W.; Szotek, Z.; Temmerman, W. M.; Ernst, A.; Hoffmann, M.; Hergert, W.; Muñoz, M. C. Ab Initio Study of the *p*-Hole Magnetism at Polar Surfaces of ZnO: The Role of Correlations. *J. Phys.: Condens. Matter* **2016**, *28*, 016003.
- (23) Coey, M.; Ackland, K.; Venkatesan, M.; Sen, S. Collective Magnetic Response of CeO₂ Nanoparticles. *Nat. Phys.* **2016**, *12*, 694–699.
- (24) Kaewmaraya, T.; Pathak, B.; Araujo, C. M.; Rosa, A. L.; Ahuja, R. Water Adsorption on ZnO(1010): The Role of Intrinsic Defects. *Europhys. Lett.* **2012**, *97*, 17014.
- (25) Giacopetti, L.; Satta, A. Degradation of Cd-Yellow Paints: Ab Initio Study Of Native Defects in 10.0 Surface CdS. *Microchem. J.* **2016**, *126*, 214–219.
- (26) Giacopetti, L.; Satta, A. Degradation of Cd-Yellow Paints: Ab Initio Study of the Adsorption of Oxygen and Water on 10.0 CdS Surface. *J. Phys.: Conf. Ser.* **2014**, *566*, 012021.
- (27) Kohn, W.; Sham, L. J. Self-Consistent Equations Including Exchange and Correlation Effects. *Phys. Rev.* **1965**, *140*, A1133–A1138.
- (28) Kresse, G.; Furthmüller, J. Efficiency of Ab-Initio Total Energy Calculations For Metals and Semiconductors Using a Plane-Wave Basis Set. *Comput. Mater. Sci.* **1996**, *6*, 15–50.
- (29) Kresse, G.; Furthmüller, J. Efficient Iterative Schemes for Ab Initio Total-Energy Calculations Using a Plane-Wave Basis Set. *Phys. Rev. B: Condens. Matter Mater. Phys.* **1996**, *54*, 11169–11186.
- (30) Nishidate, K.; Sato, T.; Matsukura, Y.; Baba, M.; Hasegawa, M.; Sasaki, T. Density-Functional Electronic Structure Calculations for Native Defects and Cu Impurities in CdS. *Phys. Rev. B: Condens. Matter Mater. Phys.* **2006**, *74*, 035210.
- (31) Adachi, S. *Properties of Group-IV, III-V and II-VI Semiconductors*; John Wiley & Sons, Ltd.: New York, 2005; pp 1–21.
- (32) Perdew, J. P.; Burke, K.; Ernzerhof, M. Generalized Gradient Approximation Made Simple. *Phys. Rev. Lett.* **1996**, *77*, 3865–3868.
- (33) Klimes, J.; Bowler, D. R.; Michaelides, A. Chemical Accuracy for the Van Der Waals Density Functional. *J. Phys.: Condens. Matter* **2010**, *22*, 022201.
- (34) Klimes, J.; Bowler, D. R.; Michaelides, A. Van der Waals Density Functionals Applied to Solids. *Phys. Rev. B: Condens. Matter Mater. Phys.* **2011**, *83*, 195131.
- (35) Wei, S.-H.; Zunger, A. Role of Metal *D* States in II-VI Semiconductors. *Phys. Rev. B: Condens. Matter Mater. Phys.* **1988**, *37*, 8958–8981.
- (36) Dudarev, S. L.; Botton, G. A.; Savrasov, S. Y.; Humphreys, C. J.; Sutton, A. P. Electron-Energy-Loss Spectra and the Structural Stability of Nickel Oxide: An LSDA+U Study. *Phys. Rev. B: Condens. Matter Mater. Phys.* **1998**, *57*, 1505–1509.
- (37) Vesely, C. J.; Hengehold, R. L.; Langer, D. W. Uv Photoemission Measurements of the Upper *D* Levels in the IIB-VIA Compounds. *Phys. Rev. B* **1972**, *5*, 2296–2301.
- (38) Monkhorst, H. J.; Pack, J. D. Special Points For Brillouin-Zone Integrations. *Phys. Rev. B* **1976**, *13*, 5188–5192.
- (39) Lany, S. Semiconductor Thermochemistry in Density Functional Calculations. *Phys. Rev. B: Condens. Matter Mater. Phys.* **2008**, *78*, 245207.
- (40) Implementation of Van der Waals Density Functional Approach to the Spin-Polarized System: Interaction Potential between Oxygen Molecules. *J. Phys. Soc. Jpn.* **2013**, *82*, 093701.